SCIENCE CHINA
Technological Sciences

• Article •

July 2015 Vol.58 No.7: 1125–1136
doi: 10.1007/s11431-015-5831-2

A particle-breakage critical state model for rockfill material

XIAO Yang[1,2*], SUN YiFei[3] & HANIF Khairul Fikry[4]

[1] Key Laboratory of New Technology for Construction of Cities in Mountain Area, Chongqing University, Chongqing 400045, China;
[2] College of Civil Engineering, Chongqing University, Chongqing 400045, China;
[3] Faculty of Engineering and Information Sciences, University of Wollongong, Wollongong 2522, Australia;
[4] Faculty of Engineering, Computing and Mathematics, University of Western Australia, Perth 6907, Australia

Received February 17, 2015; accepted April 28, 2015; published online May 22, 2015

Particle breakage has a significant influence on the stress-strain and strength behavior of rockfill material. A breakage critical state theory (BCST) was proposed to describe the evolution of particle breakage. The breakage critical state line in the breakage critical state theory was correlated with the breakage factor, which was fundamentally different from that of the original critical state theory. A simple elastoplastic constitutive model was developed for rockfill in the frame of BCST. An associated flow rule was adopted in this model. Isotropic, contractive and distortional hardening rules were suggested in view of the particle breakage. It was observed that the proposed model could well represent the complex deformation behaviors of rockfill material, such as the strain hardening, post-peak strain softening, volumetric contraction, volumetric expansion, and particle breakage under different initial confining pressures.

rockfill material, particle breakage, critical state theory, hardening rule, constitutive model

Citation: Xiao Y, Sun Y F, Hanit K F. A particle-breakage critical state model for rockfill material. Sci China Tech Sci, 2015, 58: 1125–1136, doi: 10.1007/s11431-015-5831-2

1 Introduction

Mechanical responses of rockfill material to external loading are mainly governed by the inter-particle sliding, rolling and breakage. Unlike the damage evolutions of frozen soil [1], concrete [2], and sandwich structures [3], rockfill material exhibits particle breakage as a result of the large confining pressure, cyclic loading, and wetting. As shown in many triaxial test results [4–13], particle breakage has a significant influence on the stress-strain and strength behaviors of rockfill material. To investigate the influence of particle breakage on the mechanical responses of granular aggregates, lots of breakage indices have been proposed. However, most of the particle breakage indices [4,14–18] rely on the determination of particle size distributions before and after tests. Miura et al. [19] used increments of fines content (75 μm or less) induced during consolidation and shearing process as the breakage index. The increase of particle-surface area and the fractal distribution of the newly generated smaller-sized particles during loading were also adopted to quantify the degree of particle breakage [20–28].

Many constitutive models were proposed to capture the stress-strain behavior of rockfill material, including (a) hyperbolic models [29,30]; (b) elastoplastic constitutive models [31,32]; (c) hypoplastic constitutive models [33–35]; (d) and specific constitutive models [36–38]. However, these models cannot take into account the influence of particle breakage on the stress-strain behaviors unless they are fully extended. To incorporate the effect of particle breakage, many different models were proposed, for example, models [7,8] based on the disturbed state concept (DSC) [39,40], the modified hardening parameters [41,42], and the bound-

*Corresponding author (email: hhuxyanson@163.com)

© Science China Press and Springer-Verlag Berlin Heidelberg 2015

ing surface plasticity [43–46]. However, these models cannot represent the evolution of the particle size distribution in the whole process of shearing.

Critical state theory (CST) [47,48] is a landmark of the modern soil mechanics. Most of the constitutive models [49,50] for soils were established based on this theory. However, particle was supposed to slide, rotate, but not crush in the classical CST. Unfortunately, particle size distribution (PSD) of soil usually shifts due to particle crushing, which could lead to the change of the critical state line (CSL). Russell and Khalili [51] established a bounding surface model incorporating a three-segment type CSL in the e-ln$p$ (void ratio versus mean effective stress in log scale) plane to describe the behavior of crushable granular materials. Daouadji et al. [52,53] formed a relationship between the position of CSL and the amount of energy needed for particle breakage, and affirmed that the CSL in the e-ln$p$ descended according to the evolution of PSD. Muir Wood and Maeda [54] thought that the constitutive model could incorporate the evolution of PSD as a model state parameter. This state parameter is similar to that proposed by Einav [27,28]. A series of critical state lines resulting from particle crushing compose a critical state surface [54]. Laboratory tests [51,55–57] show that the slope of CSL for sands in the p-q (mean effective stress versus deviatoric stress) plane is independent of particle breakage. However, the large-scale triaxial experimental results of rockfill material [58–60] indicate that the slope of CSL in p-q plane is nonlinear and dependent on the confining pressure because of particle breakage. CSL is supposed to be unique in CST, however, this is not suitable for soils exhibiting particle breakage.

Two kinds of relative breakage factors are introduced based on the research [27,28]. A breakage critical state theory (BCST) is proposed for rockfill material. Then, a simple constitutive model in the framework of BCST is established to reproduce the breakage and stress-strain behaviors for rockfill material.

2 Relative particle breakage

Einav [27,28] used the fractal theory to modify the relative breakage proposed by Hardin [15]. This concept may cause different values of relative breakage at the same stress point with different stress paths. To avoid this, two relative breakage factors are defined: (a) B_r^u the relative particle breakage factor at the ultimate state; (b) B_r^{cr} the relative particle breakage factor at the critical state. B_r^u is used in different shear processes while B_r^{cr} is only applied in one shear process.

The relative breakage defined by Einav [27,28] can be expressed as follows:

$$B_r = \frac{\int_{d_m}^{d_M} \left(F(d) - F_0(d)\right) d^{-1}\mathrm{d}d}{\int_{d_m}^{d_M} \left(F_u(d) - F_0(d)\right) d^{-1}\mathrm{d}d}, \tag{1}$$

where d_m is the smallest particle size; d_M is the largest particle size.

Based on these fractal researches by McDowell et al. [61], the present particle-size distribution $F(d)$ in eq. (1), i.e., a cumulative distribution by mass can be expressed as follows:

$$F(d) = PSD(\delta < d) = \left(\frac{d}{d_M}\right)^{3-\alpha}, \tag{2}$$

where α is the fractal dimension; δ is a parameter describing the particle size; d is the present particle size.

The particle size distribution at the initial state $F_0(d)$ is expressed as follows:

$$F_0(d) = \left(\frac{d}{d_M}\right)^{3-\alpha_0}, \tag{3}$$

where α_0 is the initial fractal dimension. α_0 can be obtained from the initial particle size distribution of rockfill material.

The particle size distribution at the ultimate state $F_u(d)$ is expressed as follows:

$$F_u(d) = \left(\frac{d}{d_M}\right)^{3-\alpha_u}, \tag{4}$$

where α_u is the fractal dimension at the ultimate state.

The particle size distribution at the critical state $F_{cr}(d)$ is expressed as follows:

$$F_{cr}(d) = \left(\frac{d}{d_M}\right)^{3-\alpha_{cr}}, \tag{5}$$

where α_{cr} is the fractal dimension at the critical state.

In this paper, two relative breakage factors are defined. Combinations of eqs. (1)–(4) gives a relative particle breakage factor B_r^u at the ultimate state as follows:

$$B_r^u = \frac{(\alpha - \alpha_0)(3 - \alpha_u)}{(\alpha_u - \alpha_0)(3 - \alpha)}. \tag{6}$$

Substitution of $F_u(d)$ with $F_{cr}(d)$ in eq. (1) gives a relative particle breakage factor B_r^{cr} at the critical state as follows:

$$B_r^{cr} = \frac{(\alpha - \alpha_0)(3 - \alpha_{cr})}{(\alpha_{cr} - \alpha_0)(3 - \alpha)}. \tag{7}$$

The fractal dimension at critical states changes with the magnitude of stress. The fractal dimension at the ultimate state is invariant for the same material. The relative breakage at the critical state bears a physical meaning, which indicates the degree of particle breakage in the process of shearing. The relative breakage at the ultimate state also has a physical meaning of the magnitude of particle breakage in the state of shearing relative to the ultimate state. The relationship between relative breakages at the critical and ultimate states is deduced from eqs. (6) and (7) as follows:

$$B_u^{cr}=\frac{B_r^{cr}}{B_r^{u}}=\frac{\left(3-\alpha_{cr}\right)\left(\alpha_u-\alpha_0\right)}{\left(3-\alpha_u\right)\left(\alpha_{cr}-\alpha_0\right)}. \tag{8}$$

Combination of eqs. (2) and (6) gives PSD as a function of B_r^u as follows:

$$F\left(d\right)=PSD\left(\delta<d\right)=\left(\frac{d}{d_M}\right)^{3-\frac{\alpha_u\left(3B_r^u-\alpha_0\right)+\alpha_0\left(3-3B_r^u\right)}{\alpha_u\left(B_r^u-1\right)+\left(3-\alpha_0 B_r^u\right)}}. \tag{9}$$

Figure 1 shows the variation of PSD due to the relative particle breakage factor B_r^u at the ultimate state. The fractal dimension at the breakage critical state is correlated with the initial confining pressure as follows:

$$\alpha_{cr}=\alpha_0+\left(\alpha_u-\alpha_0\right)\frac{p_{ini}/p_a}{k_\alpha+p_{ini}/p_a}, \tag{10}$$

where k_α is a material parameter; p_{ini} is the initial confining pressure; p_a is the atmosphere pressure.

Eq. (10) illustrates that the fractal dimension increases with the increase of initial confining pressure, indicating that the degree of particle crushing increases with the increase of initial confining pressure.

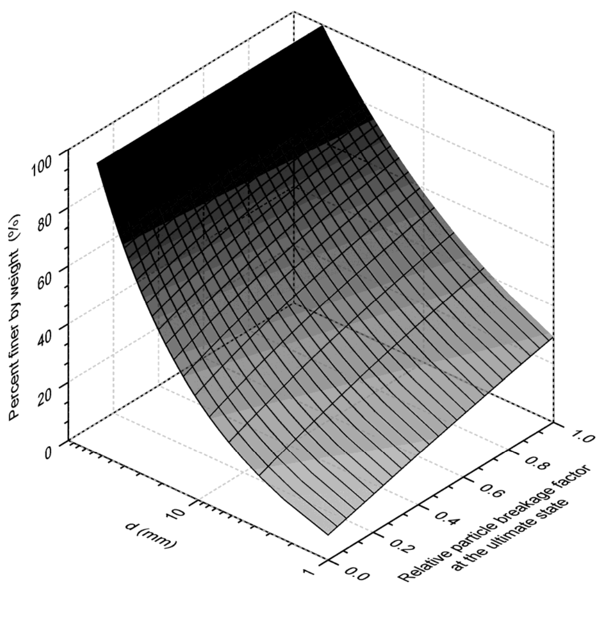

Figure 1 Particle size distribution related to the relative particle breakage factor.

It is fundamentally significant to find out the evolution rule of the relative particle breakage factor. The relative particle breakage factor B_r^{cr} at the critical state is assumed to be correlated with the accumulated strain as follows:

$$B_r^{cr}=1-\exp\left(-k_B\varepsilon_B\right), \tag{11}$$

$$\varepsilon_B=\left(\varepsilon_{ij}^p\varepsilon_{ij}^p\right)^{1/2}, \tag{12}$$

where k_B is a material parameter.

The strain parameter ε_B in the multi-principal stress space can be rewritten as

$$\varepsilon_B=\sqrt{\frac{1}{3}\left(\varepsilon_v^p\right)^2+\frac{3}{2}\left(\varepsilon_s^p\right)^2}. \tag{13}$$

Differentiation of eq. (11) gives

$$\mathrm{d}B_r^{cr}=\frac{\left(1-B_r^{cr}\right)k_B}{\varepsilon_B}\left(\frac{1}{3}\varepsilon_v^p\mathrm{d}\varepsilon_v^p+\frac{3}{2}\varepsilon_s^p\mathrm{d}\varepsilon_s^p\right). \tag{14}$$

Eq. (14) is important for the evolution of hardening rule in establishing a constitutive model.

3 Breakage critical state theory (BCST)

CST cannot reflect the evolution of particle breakage. CSL in both *e*-ln*p* and *p*-*q* planes is supposed to be unique in CST. Breakage critical sate theory (BCST) can take into account particle crushing by adding a breakage factor into *e*-ln*p* or *p*-*q* planes. It is supposed that the current breakage, strain and stress tend to be steady at the breakage critical state. The sufficient conditions for a breakage critical state are given as follows:

$$B_r^{cr}=1, \tag{15}$$

$$\eta=M_{cr}^B, \tag{16}$$

$$e=e_{cr}, \tag{17}$$

where e is a void ratio; e_{cr} is a void ratio at the critical state; η is a stress ratio of the deviatoric stress q to the mean stress p; M_{cr}^B is the slope of the breakage critical state line in the *p*-*q* plane.

The relative particle breakage factor B_r^{cr} at the critical state always equals unit even under different stress paths, while the relative particle breakage factor B_r^u at the ultimate state changes with stress path as indicated in eqs. (6)–(8). Both B_r^{cr} and B_r^u are the same as the one at final ultimate sate. Therefore, the particle size distribution (PSD) at critical sates in different stress paths is related to B_r^u. And the breakage critical state line (BCSL) is also correlated with B_r^u.

As shown in Figure 2(a), the slope of BCSL in the *p*-*q* plane is correlated with the relative particle breakage factor B_r^u at the ultimate state.

$$M_{cr}^B = \frac{q_{cr}}{p_{cr}}, \tag{18}$$

$$M_{cr}^B = M_{cr}^0 \exp\left(-k_M B_r^u\right), \tag{19}$$

where q_{cr} is the deviatoric stress at the critical state; p_{cr} is the mean effective stress at the critical state; M_{cr}^0 and k_M are model parameters.

As shown in Figure 2(b), the slope of BCSL in the *e*-ln*p* plane is defined as a function of the relative particle breakage factor B_r^u at the ultimate state.

$$e_{cr} = e_{cr}^0 - \lambda_B \ln p, \tag{20}$$

$$\lambda_B = \lambda_B^0 \exp\left(k_\lambda B_r^u\right), \tag{21}$$

where e_{cr}^0 is the initial void ratio at the critical state; λ_B is the slope of the breakage critical state line in the *e*-ln*p* plane; λ_B^0 and k_λ are model parameters.

The parameter λ_B^0 is correlated with the initial confining pressure, which can be predicted with a power function as follows:

$$\lambda_B^0 = \chi_B \left(\frac{p_{ini}}{p_a}\right)^n, \tag{22}$$

where χ_B and n are model parameters.

Figure 2(a) illustrates that the slope of BCSL M_{cr}^B in the *p*-*q* plane decreases with the increase of relative particle breakage factor B_r^u at the ultimate state, while the slope of BCSL λ_B in the *e*-ln*p* plane, as shown in Figure 2(b), increases with the increase of B_r^u.

4 Yielding surface

An elliptic surface in Figure 3 is used as a yielding surface, the equation of which can be expressed as follows:

$$\begin{aligned} f = &\left(M_{cr}^B\right)^2 \beta^2 \left(p - \beta p_0\right)^2 + \left(1-\beta\right)^2 q^2 \\ &- \left(M_{cr}^B\right)^2 \beta^2 \left(1-\beta\right)^2 p_0^2 = 0, \end{aligned} \tag{23}$$

where the ellipsoidal aspect ratio β controls the shape of the yielding surface; p_0 is actually a hardening parameter, which controls the size of the yielding surface. Figure 3 only shows half surface with the deviatoric stress larger than zero.

In general, the mean effective stress p and deviatoric stress q in eq. (23) can be defined as follows:

$$p = \frac{1}{3}\sigma_{ij}\delta_{ij}, \tag{24}$$

$$q = \sqrt{\frac{3}{2} S_{ij} S_{ij}}, \tag{25}$$

$$S_{ij} = \sigma_{ij} - p\delta_{ij}, \tag{26}$$

where δ_{ij}, the Kronecker's delta, is defined as follows:

$$\delta_{ij} = \begin{cases} 1, & i = j, \\ 0, & i \neq j. \end{cases} \tag{27}$$

The mean effective stress p and deviatoric stress q can be expressed by a scalar ρ as follows:

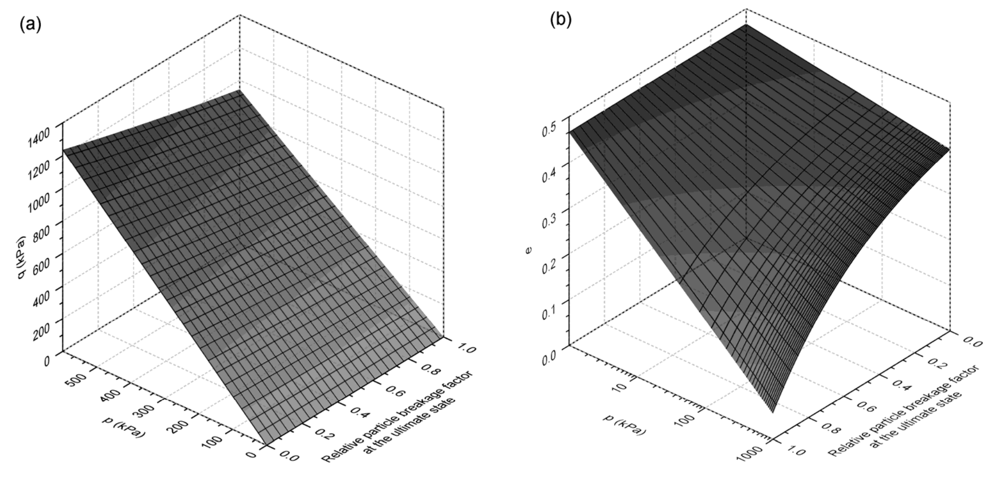

Figure 2 (a) Breakage critical state line in *p*-*q* plane related to the relative particle breakage factor; (b) breakage critical state line in *e*-ln*p* plane related to the relative particle breakage factor.

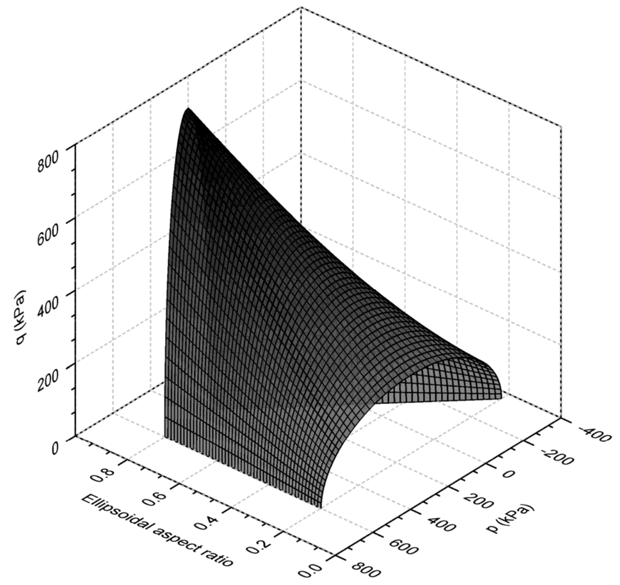

Figure 3 Elliptic yielding surface.

$$p = \rho p_0 , \tag{28}$$

$$q = \rho \eta p_0 , \tag{29}$$

where η is a ratio of the deviatoric stress q to the mean effective stress p.

Substitution of eqs. (28) and (29) into eq. (23) gives

$$\rho = \frac{\left(M_{cr}^B\right)^2 \beta^3}{\left(M_{cr}^B\right)^2 \beta^2 + \eta^2 (1-\beta)^2} + \frac{\sqrt{\left(M_{cr}^B\right)^4 \beta^6 - \left(M_{cr}^B\right)^2 \beta^2 (2\beta - 1)\left[\left(M_{cr}^B\right)^2 \beta^2 + \eta^2 (1-\beta)^2\right]}}{\left(M_{cr}^B\right)^2 \beta^2 + \eta^2 (1-\beta)^2} . \tag{30}$$

5 Hardening rule

The isotropic, contractive and distortional hardening rules are introduced in this part. The isotropic and contractive hardening rules are used to control the size of yielding surface, while the distortional hardening rule can determine the shape of yielding surface. An associated flow rule is adopted in the hardening.

5.1 Isotropic hardening rule

Usually the yielding surface expands, contracts, or remains unchanged in size depending on the plastic volumetric strain rate. Similar to that in the modified Cam-Clay model [48], the evolution of p_0 is determined by the plastic volumetric:

$$p_0 = p_0 \mathrm{e}^{\frac{1+e_0}{\lambda_B - \kappa}\varepsilon_v^p} . \tag{31}$$

Differentiation of eq. (31) with respect to ε_v^p gives

$$\frac{\partial p_0}{\partial \varepsilon_v^p} = p_0 \frac{1+e_0}{\lambda_B - \kappa} . \tag{32}$$

5.2 Contractive hardening rule

The development of the size of the yielding surface is not only depended on the incremental plastic volumetric strain but also the parameter λ_B, which is included in the function of p_0. And, the parameter λ_B is also correlated with the relative particle breakage factor B_r^{cr} at the critical state.

Combination of eqs. (8) and (14) gives

$$\begin{aligned} \mathrm{d}B_r^u &= \frac{\partial B_r^u}{\partial B_r^{cr}} \frac{\partial B_r^{cr}}{\partial \varepsilon_v^p} \mathrm{d}\varepsilon_v^p + \frac{\partial B_r^u}{\partial B_r^{cr}} \frac{\partial B_r^{cr}}{\partial \varepsilon_s^p} \mathrm{d}\varepsilon_s^p \\ &= \frac{k_B \left(1 - B_r^{cr}\right)}{\varepsilon_B B_u^{cr}} \left(\frac{1}{3} \varepsilon_v^p \mathrm{d}\varepsilon_v^p + \frac{3}{2} \varepsilon_s^p \mathrm{d}\varepsilon_s^p \right). \end{aligned} \tag{33}$$

Combination of eqs. (21) and (33) gives

$$\begin{aligned} \mathrm{d}\lambda_B &= \frac{\partial \lambda_B}{\partial B_r^u} \mathrm{d}B_r^u \\ &= \frac{k_\lambda k_B \lambda_B \left(1 - B_r^{cr}\right)}{\varepsilon_B B_u^{cr}} \left(\frac{1}{3} \varepsilon_v^p \mathrm{d}\varepsilon_v^p + \frac{3}{2} \varepsilon_s^p \mathrm{d}\varepsilon_s^p \right). \end{aligned} \tag{34}$$

Differentiation of eq. (31) with respect to λ_B gives

$$\frac{\partial p_0}{\partial \lambda_B} = -p_0 \frac{(1+e_0)\varepsilon_v^p}{(\lambda_B - \kappa)^2} . \tag{35}$$

It can be seen from eq. (35) that p_0 decreases with the increase of plastic volumetric strain.

Combination of eqs. (32), (34) and (35) gives

$$\begin{aligned} \mathrm{d}p_0 = & p_0 \frac{1+e_0}{\lambda_B - \kappa} \mathrm{d}\varepsilon_v^p - p_0 k_\lambda k_B \lambda_B \frac{(1+e_0)}{(\lambda_B - \kappa)^2} \\ & \times \frac{\left(1 - B_r^{cr}\right)}{B_u^{cr}} \frac{\varepsilon_v^p}{\varepsilon_B} \left(\frac{1}{3} \varepsilon_v^p \mathrm{d}\varepsilon_v^p + \frac{3}{2} \varepsilon_s^p \mathrm{d}\varepsilon_s^p \right). \end{aligned} \tag{36}$$

5.3 Distortional hardening rule

The slope (M_{cr}^B) of the BCSL in the p-q plane controls the ratio of q versus p in the yielding surface. The top point on the yielding surface declines with the decrease of M_{cr}^B when given the values of p_0. The following equation is used for distortional hardening:

$$\mathrm{d}M_{cr}^{B} = \frac{\partial M_{cr}^{B}}{\partial B_{r}^{u}} \mathrm{d}B_{r}^{u} . \tag{37}$$

Substitution of eqs. (19) and (33) into eq. (37) gives

$$\mathrm{d}M_{cr}^{B} = -\frac{k_M k_B M_{cr}^{B}\left(1-B_r^{cr}\right)}{\varepsilon_B B_u^{cr}}\left(\frac{1}{3}\varepsilon_v^p \mathrm{d}\varepsilon_v^p + \frac{3}{2}\varepsilon_s^p \mathrm{d}\varepsilon_s^p\right). \tag{38}$$

Eq. (38) indicates that the slope of the BCSL in the p-q plane decreases with the increase of plastic volumetric strain.

The model obeys the associated flow rule. Thus the yielding function also serves as the plastic potential function. The incremental plastic strain is determined as

$$\mathrm{d}\varepsilon_{ij}^{p} = \mathrm{d}\lambda \frac{\partial f}{\partial \sigma_{ij}} , \tag{39}$$

where the plastic index dλ is determined as

$$\mathrm{d}\lambda = \frac{1}{A_p}\frac{\partial f}{\partial \sigma_{ij}} \mathrm{d}\sigma_{ij} . \tag{40}$$

The consistency condition of the yielding function can be obtained as

$$\frac{\partial f}{\partial \sigma_{ij}}\mathrm{d}\sigma_{ij} + \frac{\partial f}{\partial p_0}\mathrm{d}p_0 + \frac{\partial f}{\partial M_r^u}\mathrm{d}M_r^u = 0 . \tag{41}$$

Therefore, the plastic modulus A_p can be obtained by combining eqs. (36), (38)–(41) as follows:

$$\begin{aligned} A_p = & -\frac{\partial f}{\partial p_0}\frac{\partial p_0}{\partial \lambda_B}\frac{\partial \lambda_B}{\partial B_r^u}\frac{\partial B_r^u}{\partial B_r^{cr}}\left(\frac{\partial B_r^{cr}}{\partial \varepsilon_v^p}\frac{\partial f}{\partial p} + \frac{\partial B_r^{cr}}{\partial \varepsilon_s^p}\frac{\partial f}{\partial q}\right) \\ & -\frac{\partial f}{\partial M_{cr}^B}\frac{\partial M_{cr}^B}{\partial B_r^u}\frac{\partial B_r^u}{\partial B_r^{cr}}\left(\frac{\partial B_r^{cr}}{\partial \varepsilon_v^p}\frac{\partial f}{\partial p} + \frac{\partial B_r^{cr}}{\partial \varepsilon_s^p}\frac{\partial f}{\partial q}\right) \\ & -\frac{\partial f}{\partial p_0}\frac{\partial p_0}{\partial \varepsilon_v^p}\frac{\partial f}{\partial p} \\ = & \frac{\partial f}{\partial p_0}\frac{p_0 k_\lambda k_B \lambda_B\left(1+e_0\right)}{\left(\lambda_B-\kappa\right)^2}\frac{\left(1-B_r^{cr}\right)}{B_u^{cr}}\frac{\varepsilon_v^p}{\varepsilon_B} \\ & \times\left(\frac{1}{3}\varepsilon_v^p\frac{\partial f}{\partial p} + \frac{3}{2}\varepsilon_s^p\frac{\partial f}{\partial q}\right) + \frac{\partial f}{\partial M_{cr}^B} \\ & \times\frac{\left(1-B_r^{cr}\right)}{B_u^{cr}}\frac{k_M k_B M_{cr}^B}{\varepsilon_B}\left(\frac{1}{3}\varepsilon_v^p\frac{\partial f}{\partial p} + \frac{3}{2}\varepsilon_s^p\frac{\partial f}{\partial q}\right) \\ & -\frac{\partial f}{\partial p_0}\frac{\partial f}{\partial p}\frac{p_0\left(1+e_0\right)}{\lambda_B-\kappa}, \end{aligned} \tag{42}$$

where

$$\frac{\partial f}{\partial p_0} = -2p_0\left(M_{cr}^B\right)^2\beta^2\left[\beta\left(\rho-\beta\right)+\left(1-\beta\right)^2\right], \tag{43}$$

$$\frac{\partial f}{\partial M_{cr}^B} = 2p_0^2 M_{cr}^B \beta^2\left[\left(\rho-\beta\right)^2 - \left(1-\beta\right)^2\right]. \tag{44}$$

The plastic flow direction is normalized as a unit vector normal to the yielding surface. The components of the unit vector n_v and n_s can be given as

$$n_v = \frac{1}{L}\frac{\partial f}{\partial p}, \tag{45}$$

$$n_s = \frac{1}{L}\frac{\partial f}{\partial q}, \tag{46}$$

where

$$\frac{\partial f}{\partial p} = 2p_0\left(M_{cr}^B\right)^2\beta^2\left(\rho-\beta\right), \tag{47}$$

$$\frac{\partial f}{\partial q} = 2p_0\rho\left(1-\beta\right)^2\eta . \tag{48}$$

The gradient amplitude L in eqs. (45) and (46) can be expressed as follows:

$$L = \sqrt{\left(\frac{\partial f}{\partial p}\right)^2 + \left(\frac{\partial f}{\partial q}\right)^2} . \tag{49}$$

The gradient amplitude can be explicitly rewritten by substituting eqs. (47) and (48) into eq. (49) as follows:

$$L = 2p_0\sqrt{\left(M_{cr}^B\right)^4\beta^4\left(\rho-\beta\right)^2 + \rho^2\left(1-\beta\right)^4\eta^2} . \tag{50}$$

6 Constitutive equation

The total incremental strain is assumed to be composed of both elastic and plastic parts. The elastic incremental strain can be expressed as follows:

$$\mathrm{d}\varepsilon_v^e = \frac{1}{B_e}\mathrm{d}p , \tag{51}$$

$$\mathrm{d}\varepsilon_s^e = \frac{1}{3G_e}\mathrm{d}q , \tag{52}$$

where the elastic bulk modulus B_e and the elastic shear modulus G_e are defined as

$$B_e = \frac{1+e_0}{\kappa}p , \tag{53}$$

$$G_e = \frac{3\left(1-2\nu\right)}{2\left(1+\nu\right)}\frac{1+e_0}{\kappa}p , \tag{54}$$

where ν is usually set as 0.3.

The plastic incremental strain can be given as follows:

$$\mathrm{d}\varepsilon_v^p = \frac{n_v}{H}\langle n_v \mathrm{d}p + n_s \mathrm{d}q \rangle , \tag{55}$$

$$\mathrm{d}\varepsilon_s^p = \frac{n_s}{H}\langle n_v \mathrm{d}p + n_s \mathrm{d}q \rangle , \tag{56}$$

where the Macaulay bracket $\langle \ \rangle$ in eqs. (55) and (56) is defined as follows:

$$\begin{cases} \langle x \rangle = x & x > 0 , \\ \langle x \rangle = 0 & x \leqslant 0 . \end{cases} \tag{57}$$

The normalized plastic modulus H in eqs. (55) and (56) can be given as

$$H = \frac{A_p}{L^2} . \tag{58}$$

The total incremental strain can be expressed as follows:

$$\mathrm{d}\varepsilon_v = \mathrm{d}\varepsilon_v^e + \mathrm{d}\varepsilon_v^p , \tag{59}$$

$$\mathrm{d}\varepsilon_s = \mathrm{d}\varepsilon_s^e + \mathrm{d}\varepsilon_s^p . \tag{60}$$

The constitutive equation of the particle-breakage critical state model is finally established. It contains ten parameters, *i.e.*, α_u, M_{cr}^0, χ_B, n, k_α, k_M, k_B, k_λ, β and κ. The determinations of these parameters will be introduced in the next section.

7 Model parameters

The established constitutive model can predict the stress-strain behavior and the evolution of particle breakage in the process of shearing. It contains ten model parameters. They are mainly determined from the conventional triaxial tests. The values of model parameters are listed in Table 1.

The material parameter α_u is the fractal dimension at the ultimate state. α_u is invariant for rockfill material as the particle size distribution (PSD) of rockfill material tends to be steady with larger confining pressure and shear stress applied. The ultimate fractal dimension α_u for rockfill materials could be 2.7 according to [25]. The parameter β controls the shape of the yielding surface. For the sake of simplicity, β is kept as 0.50 in this paper. The swelling index κ (κ=0.0085) can be obtained from the unloading compression line in the e-ln$p$ plane.

Eq. (10) is used to reproduce the relationship between the fractal dimension and the initial confining pressure. Figure 4(a) shows that the parameter k_α in eq. (10) is supposed to be 0.35 which is in good agreement with the test data. As shown in Figure 4(b), eq. (19) is applied to predict the test results in terms of the relationship between the slope of BCSL in the p-q plane M_{cr}^B and the relative particle breakage factor B_r^u at the ultimate state. Parameters M_{cr}^0 and k_M are set as 2.80 and 0.68 for prediction. The initial slope λ_B^0 of BCSL in the e-ln$p$ plane is related to the initial confining pressure. As shown in Figure 4(c), the predictions of eq. (22) can agree well with the test results with parameters χ_B and n equal to 0.0048 and 0.68, respectively. When the parameters χ_B and n are given, the mean value of the parameter k_λ (=0.78) can be calculated by eq. (21) with values of λ_B and B_r^u obtained from tests at different initial confining pressures.

Table 1 Values of model parameters

Model prameters	Values
α_u	2.70
k_α	0.35
k_B	10.50
M_{cr}^0	2.50
k_M	0.68
k_λ	0.78
χ_B	0.48×10^{-2}
n	0.68
β	0.50
κ	0.85×10^{-2}

The parameter k_B cannot be directly determined from the conventional triaxial tests. It is difficult to evaluate the particle breakage in the whole process of shearing. Only the particle size distribution at the end of shearing is obtained. Therefore, the value of the parameter k_B has to be determined based on comparisons between the model predictions and the test results on the stress-strain relationship. This method is the same as that to determine the value of the plastic modulus introduced by Bardet [62]. The difference between the model predictions and the test results on the stress-strain relationship firstly decreases with the increase of k_B and then increases with the increase of k_B. An optimal value of k_B can make a minimal difference between the model predictions and the test results. k_B is finally determined as 10.50 for the rockfill material.

8 Model prediction

8.1 Test introduction

A series of compress tests [11] were conducted for rockfill material by the large-scale triaxial apparatus, as shown in Figure 5. The diameter and height of specimen are 300 and 600 mm, respectively. The material from Jiangsu Yixing Reservoir is a kind of quartzite sandstone containing 15% mudstone. The dry density of the aggregate in test is 2.12 g/cm^3. And, the coefficients of uniformity and curvature are 52.5 and 1.07, respectively. Table 2 presents the particle

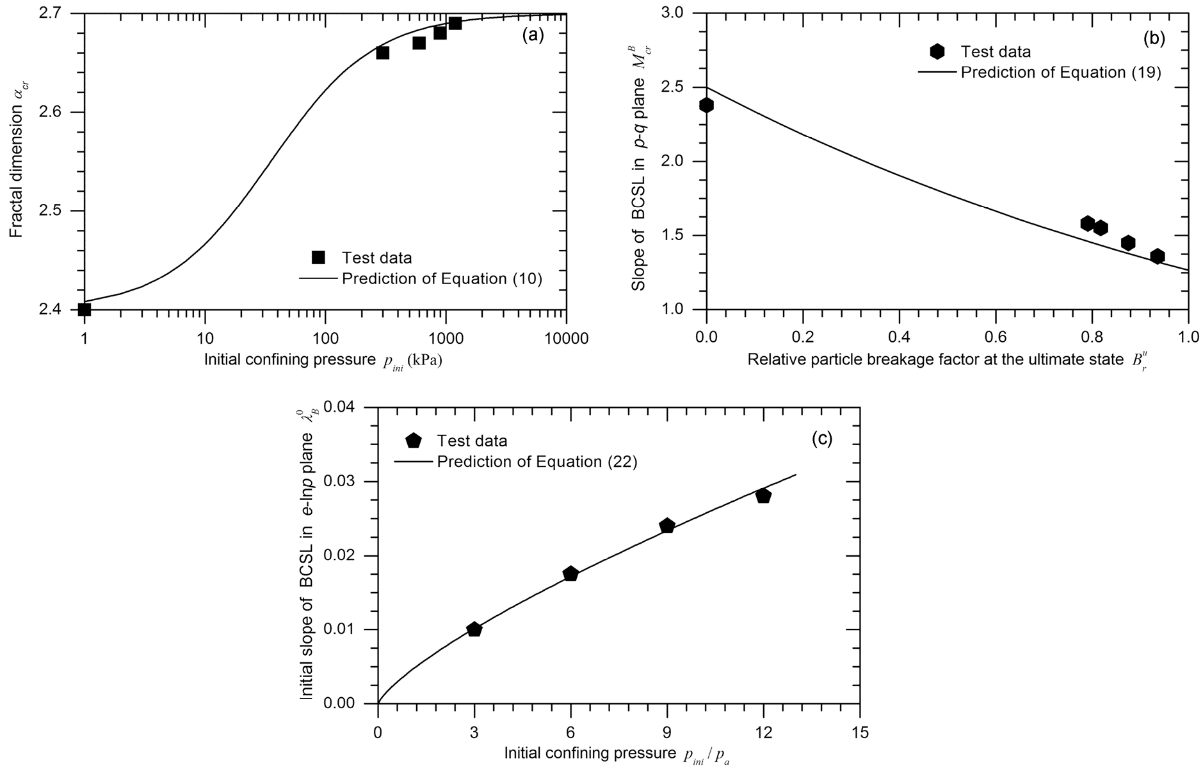

Figure 4 (a) Determination of parameter k_α; (b) determination of parameters M_{cr}^{0} and k_M; (c) determination of parameters χ_B and n.

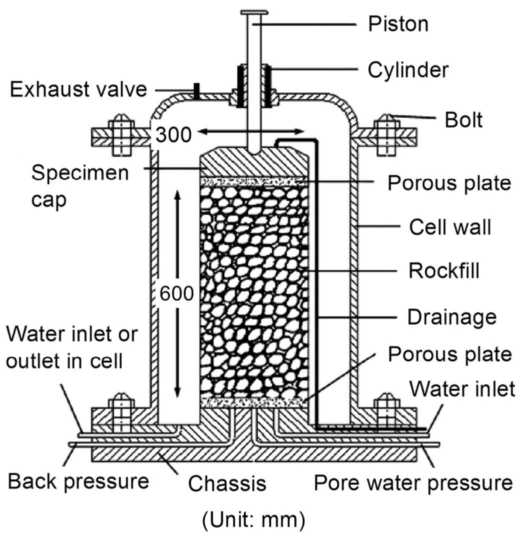

Figure 5 Large-scale triaxial apparatus.

Table 2 Particle size distribution before test

Particle size (mm)	Values (%)
0–5	19.0
5–10	14.0
10–20	22.0
20–40	30.0
40–60	15.0

size distribution before tests. The confining pressures in these tests are set as 300, 600, 900 and 1200 kPa, respectively. The axial strain increased with a rate of 2 mm/min until it increased to 15%.

8.2 Evolution of yielding surface

The constitutive model with parameters in Table 1 can reproduce the variation of the yielding surface in the process of shearing. Figure 6 shows the evolutions of yielding surfaces under different initial confining pressures. It can be seen that the big value of initial confining pressure corresponds with the large size of yielding surface. The size of yielding surface gets larger at first to the maximal one in the process of shearing. Then it becomes smaller from the maximal size. The degree of the yielding size decreasing at the end of shearing becomes smooth with the increase of initial confining pressure, which indicates that the positive dilatancy decreases with the increase of initial confining pressure. This phenomenon is mainly because that particle breakage rather than dilatancy gets dominant in the high pressure.

8.3 Prediction of stress-strain behaviors

Figure 7 illustrates the comparisons between the model predictions (solid curves) and experimental results (dots) under different initial confining pressures in the coordinate system

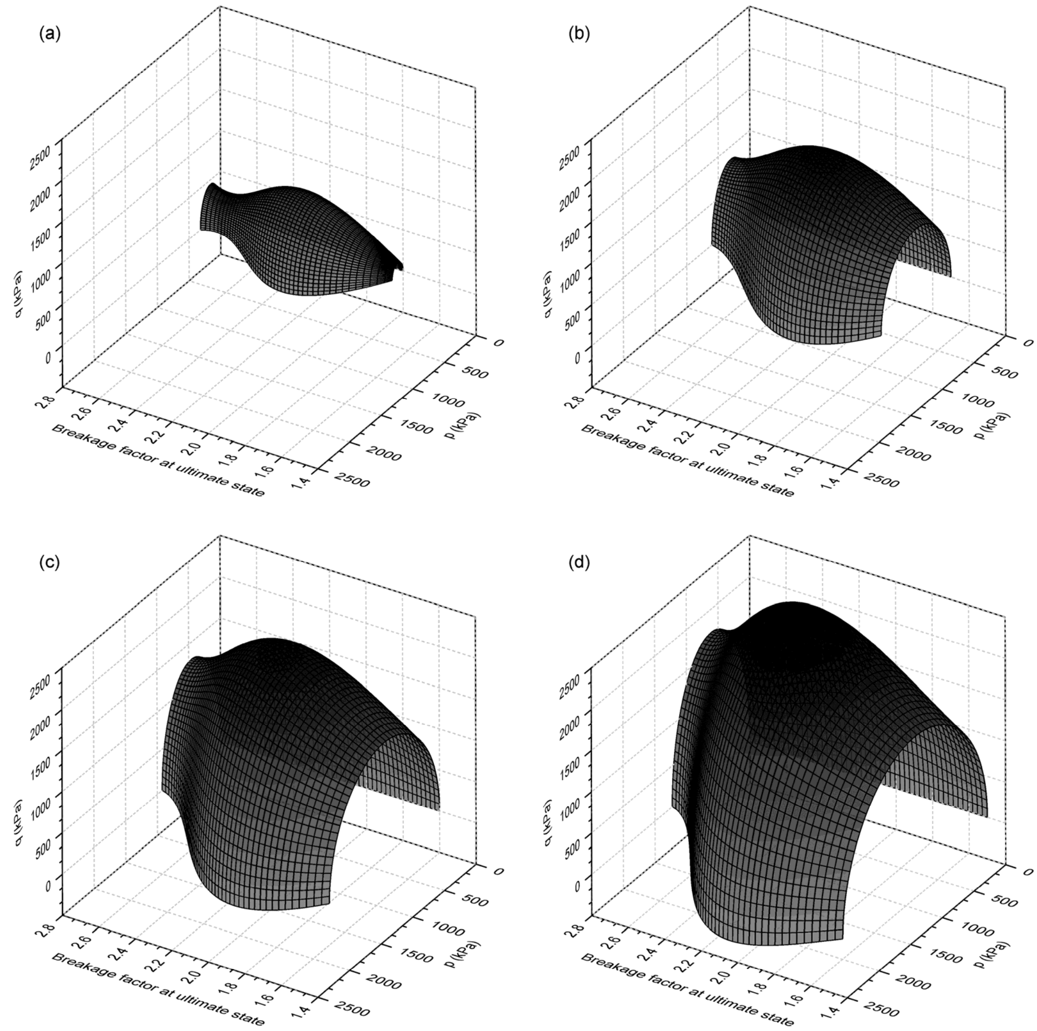

Figure 6 Evolution of yielding surface in the process of shearing: (a) p_0=300 kPa; (b) p_0=600 kPa; (c) p_0=900 kPa; (d) p_0=1200 kPa.

composed by the stress ratio, the first strain and volumetric strain. The predicted three-dimensional curves are also projected onto three planes, i.e., the stress ratio versus the first strain plane, the stress ratio versus the volumetric strain plane and the first strain versus the volumetric strain plane. The four predicted curves at each initial confining pressure can agree well with the experimental results. Rockfill material presents such behaviors as the high positive dilatancy (volumetric expansion) and the post-peak strain softening at lower initial confining pressure as shown in Figure 7(a), which indicates that the dilatancy is obvious at lower pressure. Rockfill material also presents the behaviors of volumetric contraction at high initial confining pressure as shown in Figure 7(d), which is attributed to great particle crushing at high pressure. Constitutive models based on the CST can only predict the behaviors of the strain hardening and the volumetric contraction of soils. While the constitutive model based on BCST can well predict the behaviors such as the strain hardening, the post-peak strain softening, the volumetric contraction, and the volumetric expansion.

8.4 Prediction of particle breakage

The main characteristic of this model is that it can reproduce the evolution of the particle breakage in the process of shearing, which is attributed to the breakage critical state theory proposed in this paper. The relative breakage factor embedded in the established model equations implies the development of the particle crushing in the process of shearing. The fractal dimension α is a variant. And, it can be obtained from the relative breakage factor. The fractal dimension α, based on eqs. (2) and (7), reflects the evolution of grading. As illustrated in Figure 8, the prediction of particle size distribution can agree well with the test results under different initial confining pressures.

9 Conclusions

A breakage critical sate theory (BCST) is proposed. A constitutive model based on BCST is established to reproduce

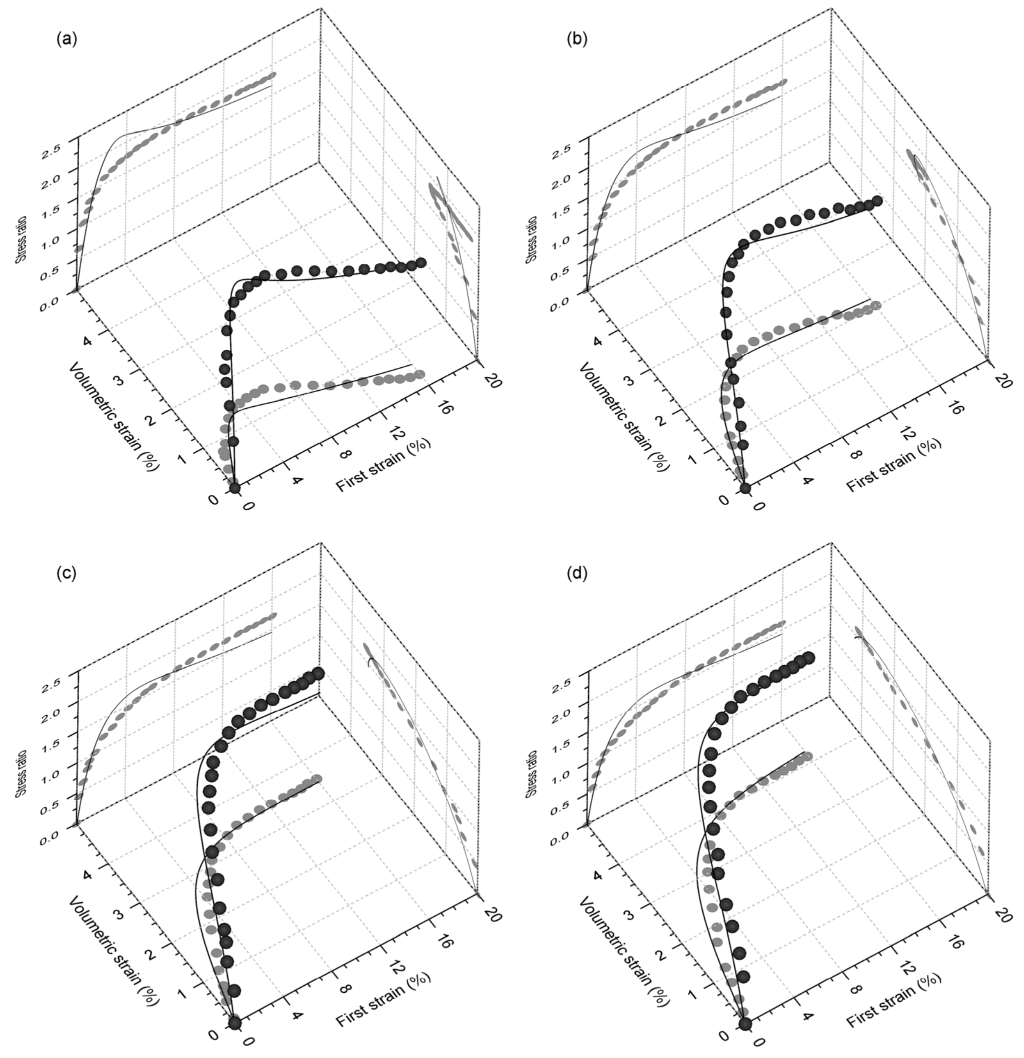

Figure 7 Relationship among stress ratio, first strain and volumetric strain: (a) p_0=300 kPa; (b) p_0=600 kPa; (c) p_0=900 kPa; (d) p_0=1200 kPa.

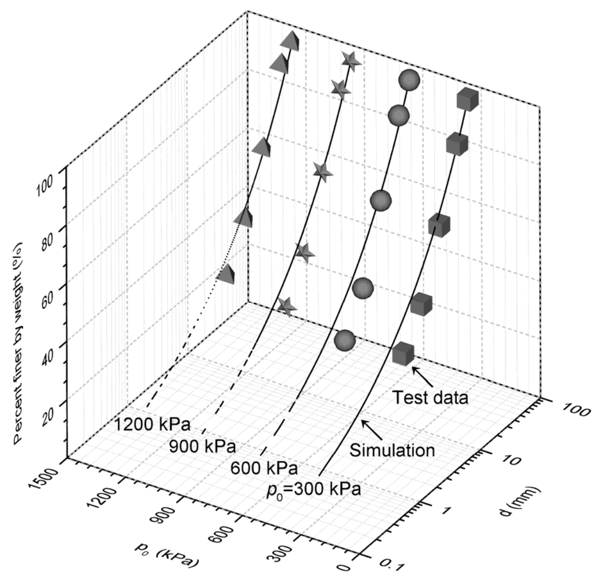

Figure 8 Evolution of particle size distribution.

the evolution of particle crushing. The main conclusions are summarized as follows.

First, two relative breakage factors were defined based on the fractal theory. The relative particle breakage factor represents how the material approached the breakage critical state. The relative particle breakage factor at the ultimate state was embedded in the equations of the breakage critical state lines. Second, the breakage critical state theory (BCST) was proposed. The breakage critical state line was correlated with the breakage factor in order to reflect the evolution of particle crushing. Sufficient conditions were given for the evaluation of a breakage critical state. Third, the constitutive model based on BCST was established. The associated flow rule was adopted for deriving model equations. Isotropic, contractive and distortional hardening rules were introduced due to evolution of particle breakage. Last, the proposed model can well predict such behaviors of rockfill material as high positive dilatancy (volumetric expansion) and the post-peak strain softening at the lower initial confining pressure. It can also describe the behaviors of volumetric contraction at high initial confining pressure. The volumetric contraction is mainly attributed to the great particle crushing at the high pressure. By incorporating the fractal breakage theory, the proposed model could also well depict the particle breakage and the associated evolution of PSD during loading.

In summary, the proposed model based on BCST can well reproduce such behaviors of rockfill materials as the strain hardening, the post-peak strain softening, the dilatancy, the particle breakage and the associated PSD evolution under different initial confining pressures.

This work was supported by the Fundamental Research Funds for the Central Universities (Grant No. 106112015CDJXY200008), and China Scholarship Council (Grant No. 201306710022).

1 Zhu Z W, Ning J G, Ma W. A constitutive model of frozen soil with damage and numerical simulation for the coupled problem. Sci China Phys Mech Astron, 2010, 53: 699–711
2 Ning J G, Liu H F, Shang L. Dynamic mechanical behavior and the constitutive model of concrete subjected to impact loadings. Sci China Phys Mech Astron, 2008, 51: 1745–1760
3 Sun S Y, Chen H R. The interfacial fracture behavior of foam core composite sandwich structures by a viscoelastic cohesive model. Sci China Phys Mech Astron, 2011, 54: 1481–1487
4 Marsal R J. Large scale testing of rockfill materials. J Soil Mech Found ASCE, 1967, 93: 27–43
5 Indraratna B, Wijewardena L S S, Balasubramaniam A S. Large-scale triaxial testing of greywacke rockfill. Géotechnique, 1993, 43: 37–51
6 Miura, S, Yangi K, Asonuma T. Deformation-strength evaluation of crushable volcanic soils by laboratory and in-situ testing. Soils Found, 2003, 43: 47–57
7 Varadarajan A, Sharma K G, Venkatachalam K, et al. Testing and modeling two rockfill materials. J Geotech Geoenviron Eng ASCE, 2003, 129: 206–218
8 Varadarajan A, Sharma K G., Abbas S M, et al. Constitutive model for rockfill materials and determination of material constants. Int J Geomech ASCE, 2006, 6: 226–237
9 Guo X L, Hu H, Bao C G. Experimental studies of the effects of grain breakage on the dilatancy and shear strength of rockfill (in Chinese). Chin J Geotech Eng, 1997, 19: 83–88
10 Xiao Y, Liu H L, Chen Y, et al. Strength and deformation of rockfill material based on large-scale triaxial compression tests. I: Influences of density and pressure. J Geotech Geoenviron Eng, 2014, 140: 04014070
11 Liu H L, Deng A, Sheng Y. Shear behavior of coarse aggregates for dam construction under varied stress paths. Water Sci Eng, 2008 ,1: 63–77
12 Honkanadavar N, Sharma K G. Testing and modeling the behavior of riverbed and blasted quarried rockfill materials. Int J Geomech, 2014, 14: 04014028
13 Liu M, Gao Y, Liu H. An elastoplastic constitutive model for rockfills incorporating energy dissipation of nonlinear friction and particle breakage. Int J Numer Anal Met, 2014, 38: 935–960
14 Fu Z, Chen S, Peng C. Modeling the cyclic behaviour of rockfill materials within the framework of generalized plasticity. Int J Geomech, 2014, 14: 191–204
15 Hardin B O. Crushing of soil particles. J Geotech Eng ASCE, 1985, 111: 1177–1192
16 Lee K L, Farhoomand I. Compressibility and crushing of granular soil. Can Geotech J, 1967, 4: 68–86
17 Lade P, Yamamuro J A, Bopp P A. Significance of particle crushing in granular materials. J Geotech Eng ASCE, 1996, 122: 309–316
18 Bai S T, Cui Y H. The mechanics characteristic of rockfill (in Chinese). J Hydroelectr Eng, 1997, 3: 21–30
19 Miura, S, Yangi K, Asonuma T. Deformation-strength evaluation of crushable volcanic soils by laboratory and *in-situ* testing. Soils Found, 2003, 43: 47–57
20 Miura N, Ohara S. Particle-crushing of a decomposed granite soils under shear stresses. Soils Found, 1979, 19: 1–14
21 Katz A J, Thompson A H. Fractal sandstone pores: implications for conductivity and pore formation. Phys Rev Lett, 1985, 54: 1325–1328
22 Turcotte D L. Fractals and fragmentation. J Geophys Res, 1986, 91: 1921–1926
23 Sun Y F, Xiao Y, Hanif K F. Compressibility dependence on grain size distribution and relative density in sands. Sci China Tech Sci, 2015, 58: 443-448.
24 McDowell G R, Bolton M D, Robertson D. The fractal crushing of granular materials. J Mech Phys Solids, 1996, 44: 2079–2102
25 Xiao Y, Liu H, Chen Y, et al. Strength and deformation of rockfill material based on large-scale triaxial compression tests. II: Influence of Particle Breakage. J Geotech Geoenviron Eng, 2014, 140: 04014071.
26 Nakata Y, Hyde A F L, Hyodo M, et al. A probabilistic approach to sand particle crushing in the triaxial test. Géotechnique, 1999, 49: 567–583
27 Einav I. Breakage mechanics–Part I: Theory. J Mech Phys Solids, 2007, 55: 1274–1297
28 Einav I. Fracture propagation in brittle granular matter. Proc R Soc A, 2007, 463: 3021–3035
29 Kulhawy F H, Duncan J M. Stresses and movements in Oroville dam. J Soil Mech Found ASCE, 1972, 98: 653–665
30 Saboya F J Jr, Byrne P M. Parameters for stress and deformation analysis of rockfill dam. Can Geotech J, 1993, 30: 690–701
31 Lade P V, Kim M K. Single hardening constitutive model for soil, rock and concrete. Int J Solids Struct, 1995, 32: 1963–1978
32 Liu H L, Xiao Y, Liu J Y, et al. A new elliptic-parabolic yield surface model revised by an adaptive criterion for granular soils. Sci China Tech Sci, 2010, 53: 2152–2159
33 Gudehus G. A comprehensive constitutive equation for granular materials. Soils Found, 1996, 36: 1–12
34 Bauer E. Hypoplastic modelling of moisture-sensitive weathered rockfill materials. Acta Geotechnica, 2009, 4: 261–272
35 Cen W J, Wang X X, Bauer E, et al. Study on hypoplastic constitutive modeling of rockfill and its application (in Chinese). Chin J Geotech Eng, 2007, 26: 312–322
36 Oldecop L A, Alonso E E. A model for rockfill compressibility. Géotechnique, 2001, 51: 127–139
37 Chu B L, Jou Y W, Weng M C. A constitutive model for gravelly soils considering shear-induced volumetric deformation. Can Geotech J, 2010, 47: 662–673
38 Araei A. A. Artificial neural networks for modeling drained monotonic behavior of rockfill materials. Int J Geomech, 2014, 14: 04014005
39 Desai C S, Toth J. Disturbed state constitutive modelling based on stress-strain and nondestructive behavior. Int J Solids Struct, 1996, 33: 1619–1650
40 Desai C S, Basaran C, Zhang W. Numerical algorithms and mesh dependence in the disturbed state concept. Int J Numer Meth Eng, 1997, 40: 3059–3083
41 Yao Y P, Yamamoto H, Wang N D. Constitutive model considering sand crushing. Soils Found, 2008, 48: 601–608
42 Sun D, Huang W, Sheng D, et al. An elastoplastic model for granular materials exhibiting particle crushing. Key Eng Mater, 2006, 340–341: 1255–1248
43 Sun Y, Xiao Y, Ju W. Bounding surface model for ballast with additional attention on the evolution of particle size distribution. Sci China Tech Sci, 2014, 57: 1352–1360
44 Xiao Y, Liu H L, Chen Y, et al. Bounding surface model for rockfill materials dependent on density and pressure under triaxial stress conditions. J Eng Mech, 2014, 140: 04014002

45 Xiao Y, Liu H, Chen Y, et al. Bounding surface plasticity model incorporating the state pressure index for rockfill materials. J Eng Mech, 2014, 140: 04014087
46 Xiao Y, Liu H L, Zhu J G, et al. Modeling and behaviours of rockfill materials in three-dimensional stress space. Sci China Tech Sci, 2012, 55: 2877–2892
47 Roscoe K H, Schofield A N, Thurairajah A. Yielding of clays in state wetter than critical. Géotechnique, 1963, 13: 211−240
48 Roscoe K H, Burland J B. On the generalized stress-strain behavior of 'wet' clay. Engineering Plasticity. Cambridge: Cambridge University Press, 1968. 535−609
49 Been K, Jefferies M G. A state parameter for sand. Géotechnique, 1985, 35: 99−112
50 Li X S, Dafalias Y F, Wang Z L. State-dependent dilatancy in critical-state constitutive modeling of sand. Can Geotech J, 1999, 36: 599−611
51 Russell A R, Khalili N. A bounding surface plasticity model for sands exhibiting particle crushing. Can Geotech J, 2004, 41: 1179–1192
52 Daouadji A, Hicher P Y. An enhanced constitutive model for crushable granular materials. Int J Numer Anal Methods Geomech, 2010, 34: 555−580
53 Daouadji A, Hicher P Y, Rahma A. An elastoplastic model for granular materials taking into account grain breakage. Eur J Mech A-Solids, 2001, 20: 113−137
54 Muir Wood D, Maeda K. Changing grading of soil: Effect on critical states. Acta Geotechnica, 2008, 3: 3−14
55 Lo K Y, Roy M. Response of particulate materials at high pressures. Soils Found, 1973, 13: 61−76
56 Yamamuro J A, Lade P V. Drained sand behaviour in axisymmetric tests at high pressures. J Geotech Eng ASCE, 1996, 122: 109−119
57 Coop M R, Sorensen K K, Bodas F T. Particle breakage during shearing of a carbonate sand. Géotechnique, 2004, 54: 157−163
58 Liu M C, Gao Y F, Huang X M. Study on elasto-plastic constitutive model of rockfills with nonlinear strength characteristics (in Chinese). Chin J Geotech Eng, 2005, 27: 294−298
59 Liu E L, Chen S S, Li G Y, et al. Critical state of rockfill materials and a constitutive model considering grain crushing (in Chinese). Rock Soil Mech, 2011, 32: 148−154
60 Ding S Y, Cai Z Y, Ling H. Strength and deformation characteristics and critical state of rock fill (in Chinese). Chin J Geotech Eng, 2010, 32: 248−252
61 McDowell G R, Bolton M D, Robertson D. The fractal crushing of granular materials. J Mech Phys Solids, 1996, 44: 2079−2102
62 Bardet J P. Bounding surface plasticity model for sands. J Eng Mech ASCE, 1986, 112: 1198–1217